Polypyrrole-doped cellulose hydrogel evaporator for steam generation and wastewater cleaning

Wang, Ruizhi; Wang, Wenxin; Jensen, Martin; Li, Xianfeng; Qiu, Honsen; Jin, Renyu; Wang, Ning

Published in:
Journal of Sol-Gel Science and Technology

DOI (link to publication from Publisher):
10.1007/s10971-023-06128-4

Publication date:
2023

Document Version
Publisher's PDF, also known as Version of record

Polypyrrole-doped cellulose hydrogel evaporator for steam generation and wastewater cleaning

Ruizhi Wang[a], Wenxin Wang[a], Martin Jensen[b], Xianfeng Li[a], Honsen Qiu[a], Renyu Jin[a], Ning Wang[a*]

a State Key Laboratory of Separation Membranes and Membrane Processes, Tianjin Municipal Key Lab of Advanced Energy Storage Material and Devices, School of Material Science and Engineering, Tiangong University, Tianjin 300387, China

b Department of Chemistry and Bioscience, Aalborg University, DK-9220 Aalborg, Denmark

E-mail: wangntjpu@hotmail.com

Abstract

Solar-driven steam generation is considered an energy-saving and environmentally friendly thermal distillation method to solve freshwater shortage through desalination and wastewater treatment. Herein, PPy-doped cellulose composite hydrogels (PCGs) are prepared for clean water production. By varying the matrix solid content, the pore structure and water transport ability of the hydrogel material can be tailored, and the water evaporation enthalpy can be reduced by creating weak hydrogen bonds. By balancing hydrophobic sites in the hydrogel, porosity induced water transport and reduced evaporation enthalpy, a water evaporation rate of 1.88 kg m^{-2} h^{-1} under one sun is obtained. Furthermore, the specific surface area and hydrophilic groups of the three-dimensional hydrogel provide adsorption sites, and the removal of methyl blue (MB) organic dye is as high as 99%. The combination of water evaporation and cleaning capabilities provide a framework for the exploration of the next generation of evaporators for wastewater treatment applications.

Key words: solar steam generation; composite hydrogels; intermediate water; photothermal conversion

Highlights

·Cellulose composite hydrogel with in-situ polymerized polypyrrole are fabricated.

·The water transport and evaporation enthalpy are balanced for water evaporation.

·The hydrogels are unaffected by salt concentrations up to 20%.

·The hydrogels are suitable for dye waste water cleaning.

1. Introduction

Water shortages are becoming increasingly prevalent across the globe and the use of natural water resources such as seawater can provide large quantities of freshwater for daily water use [1]. As an abundant and clean renewable resource, solar energy is widely used in photovoltaic cells, photocatalysis and seawater desalination [2-4]. However, traditional seawater desalination processes (e. g., reverse osmosis and multi-stage flash evaporation) are hindered by complicated preparation processes and equipment costs, or highly concentrated solutions and efficient optical materials [5, 6]. On this basis, solar-driven steam generation based on photothermal material evaporators has attracted attention as a water purification process that meets human drinking standards [7].

Direct evaporation of water under natural sunlight suffers from large heat loss and low utilization efficiency, which renders it inapplicable for scaling. Therefore, researchers have explored local evaporation processes at the air-water interface to boost the solar energy utilization efficiency [8]. Firstly, stable and efficient thermal localization effects require development of photothermal conversion materials. Currently, common light absorbing materials include deposited metal nanoparticles with plasmonic effect [9, 10], tunable absorbing semiconductor metal compounds [11-13], carbon-based materials with broad band absorption and chemical stability [7, 14, 15], and chemically synthesized nanocomposite polymers [16, 17]. Secondly, continuous and adequate water supply is paramount for solar energy efficiency, which is achievable through a two-dimensional waterway structure, created by wrapping a water absorbent material on the surface of an insulator that floats on the water surface, while the water absorbent material is in contact with the water bulk through capillary forces that continuously supply water and meanwhile inhibit heat loss [18, 19]. Unfortunately, interfacial evaporators composed of these materials are often limited by high cost, complex fabrication, low conversion efficiency, and single-function defects [20-22]. Consequently, it is relevant to explore low-cost and abundant renewable porous biomass materials, such as sugarcane [23], kapok fiber [24] and natural latex [25]. Recently, Guo et al. proposed that the introduction of renewable konjac glucomannan and black magnetic iron-based metal organic frameworks (Fe-MOF) in the PVA network can achieve efficient solar evaporation combined with heavy metal removal [26].

As the most abundant organic compound on Earth, cellulose, not only has environmental advantages and porosity, but also a high density of hydroxyl groups that can be utilized for synthesis of three-dimensional hydrophilic porous hydrogels for degradation of organic dyes and heavy metal adsorption [27-30]. Due to non-radiative relaxation phenomena and lattice vibration, hydrogels can be combined with semiconductor nanomaterials to enhance the wastewater purification ability through photocatalysis [31-33]. Further, light-absorbing materials can be embedded in the polymer network and through surface topography adjustment influencing the water state and micro-nanostructure of the gels, the thermal energy can be confined in the molecular network to reduce heat loss [34]. However, owing to the preparation complexity, such evaporators suffer from inadequate mechanical stability and unmet evaporation performance. As a result, it is desirable to rethink the design of solar evaporators with both water production and water purification capacity. It is well known that water molecules are arranged in dynamically stable water clusters through hydrogen bonding, and weakening of the hydrogen bonds in these clusters reduces the water evaporation enthalpy [35]. Thus, increasing the proportion of weakly bonded intermediate water boosts the evaporation efficiency. In addition, hydrogels can enhance solar vapor generation by tailoring the surface wettability. Guo et al. demonstrated that polyvinyl alcohol (PVA) hydrogels with surface modified hydrophobic island-like patches, possess increased water film thickness in the hydrophilic region and the enhanced contact line in the hydrophobic region ensures improved solar water evaporation, achieving an evaporation rate of 4.0 kg m^{-2} h^{-1} and an energy conversion efficiency of 93% under illumination of one sun [36].

In this work, a simple polymerization and doping method is used to prepare chemical cross-linked PPy/cellulose composite hydrogels (PCGs) for solar vapor generation. As a photothermal conductive polymer, polypyrrole (PPy) is extensively used in interfacial evaporators due to its facile preparation, full-spectrum light absorption, and easily controlled film thickness [37, 38]. The black roughness imparted by PPy to the cellulose porous framework not only enhances the hydrogel sunlight absorption, but also improves the physical adsorption capacity of the hydrogel. We investigate the thermal conductivity, water transport, and light absorption properties of the composite hydrogels by varying the solid content of the cellulose matrix.

2. Material and methods

2.1 Materials and Chemicals

Cellulose cotton linter (industrial grade) was purchased from Sanyou Group Xingda Chemical Fiber Co., Ltd (Tangshan, China). Urea (99%) was purchased from Sinopharm Chemical Reagent Co., Ltd. Pyrrole (99%) was purchased from Ailan Chemical Technology Co., Ltd (Shanghai, China). Hydrochloric acid was purchased from Kemeiou Chemical Reagent Co., Ltd (Tianjin, China). Epichlorohydrin (ECH) (99%) was purchased from Xiens Biochemical Technology Co., Ltd (Tianjin, China). Sodium hydroxide (NaOH) (99%) and ammonium persulfate (≥98%) were supplied by Fengchuan Chemical Reagent Technology Co., Ltd (Tianjin, China).

2.2 Preparation of cellulose composite hydrogels.

(1) Preparation of polypyrrole [39]. 4.56 g of ammonium persulfate was dissolved in 50 ml deionized water by ultrasonic treatment for 10 min and marked solution A. 1ml of pyrrole was poured into 50 ml of deionized water and stirred at room temperature to a form homogeneous pyrrole aqueous solution, labelled solution B. Solutions A and B were added dropwise to 100 mL of 1.2 M hydrochloric acid and transferred to a refrigerator for polymerization at 4 °C for 3 h. The reacted solution was suction filtered and washed with distilled water several times to remove impurities from the PPy particles, which were then dried in an oven at 60°C for 3 h.

(2) Preparation of PPy/cellulose hydrogels. 2.5 g of cellulose cotton linters were dissolved in 97.5 g of 7 wt% sodium hydroxide/12 wt% urea pre-cooled to -12 °C, and was then centrifuged at room temperature after freezing for 12 h to obtain a translucent cellulose solution. The PPy/cellulose mixed solutions were prepared with PPy/cellulose mass ratios of 0.01:1, 0.1:1, 0.2:1, 0.3:1 and 0.4:1, respectively. The mixed solutions were stirred in an ice bath for 1 h to obtain homogeneous solutions followed by addition of 10 g of epichlorohydrin, and black solutions were obtained after stirring for 2 h. The solutions were transferred to glass petri dishes and put into an oven at 60 °C to obtain the cellulose hydrogels, that were washed with distilled water until neutral pH to acquire PPy/cellulose hydrogels with different mass ratios, named as PCG-0.01, PCG-0.1, PCG-0.2, PCG-0.3 and PCG-0.4, respectively. In addition, the pure cellulose hydrogel material was named CG.

To explore the effect of solid content, the mass ratio of PPy and cellulose is fixed at 0.3:1, and the solid content of cellulose is set at 2.5 wt%, 3 wt%, 3.5 wt% and 4 wt%, respectively, and the other parameters unchanged, and the obtained hydrogels are named PCG1, PCG2, PCG3 and PCG4,

respectively. Figure 1 shows the preparation process of PCGs composite hydrogels.

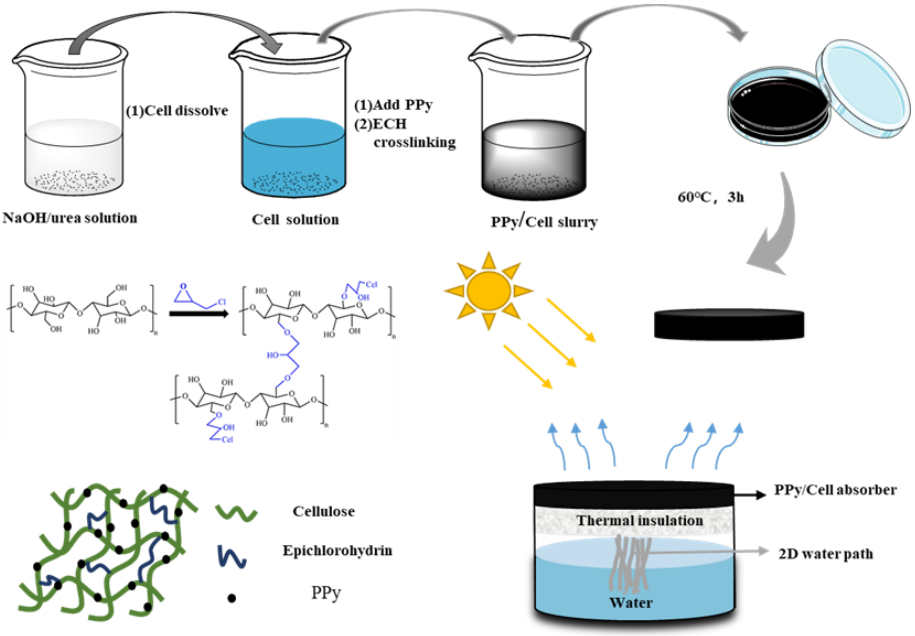

Figure 1. The preparation steps of the PPy/cellulose hydrogels.

2.3 Characterization

The microscopic morphology of the hydrogels was observed by field emission scanning electron microscopy (SEM, S-4800, Hitachis, Japan) at an accelerating voltage of 3.0 kV. Before the test, the hydrogels were freeze-dried for 12 h to remove water, and a flat section was obtained by brittle fracture in liquid nitrogen followed by gold coating. The crystal structure of the PCGs were analyzed under wet state using an X-ray diffractometer (XRD, D/MAX-2500, Japan) over a test angle range of 5º to 45º. The chemical structure of the hydrogels was analyzed by Fourier transform infrared spectrometer (FTIR, TENSOR37, Bruker, Germany) after mixing the vacuum dried hydrogels with potassium bromide at a ratio of 1:100. The measurement were performed in the spectral range of 400-4000 cm^{-1} with a resolution of 4 cm^{-1} and the presented results are an average of 16 measurements. The rheological properties of hydrogels were measured by Discovery HR-1 rheometer from TA operated in frequency scanning mode using parallel plates. The absorbance of the hydrogels in wet state was measured at a speed of 300 nm min^{-1} using a UV-Vis-NIR spectrophotometer (UH4150, HITACHI, Japan) equipped with an integrating sphere device in the wavelength range of 300-2500 nm. Baseline calibration was performed using $BaSO_4$ prior to testing. The evaporation enthalpy of the hydrogels was investigated by a differential scanning calorimeter (DSC, DSC200F3, NETZSCH, Germany). The DSC was calibrated against a sapphire

disc prior to testing. The hydrogels' surface tension is tested using an automatic contact angle measuring instrument (DAT1100) by taking 5 μL of deionized water as indicator. A thermal conductivity meter (Hot Disk, TPS 2500, Sweden) was used under wet condition to measure the thermal conductivity.

2.4 Solar evaporation experiment

The solar evaporation device is composed of a hydrogel sample (the evaporation layer) with a diameter of 60 mm and a thickness of 2 mm, and polystyrene (PS) foam and cotton as the thermal insulation layer and the water conveyance layer, respectively. The temperature in the laboratory was 25℃ and the humidity was 75%. The solar simulator (PL-XQ500W) was equipped with a built-in filter (AM 1.5G) to simulate sunlight, so that the spot size was consistent with the sample, and irradiated under one sun (1 kW m^{-2}) for 60 min. After that, the steam generation ability of the hydrogels was studied, and the water loss was monitored every 30 s by connecting the electronic balance to a computer. The temperature of the hydrogel sample surface and water were recorded using an infrared thermal imager (E4, FLIR, USA). In order to explore the ability of the PCG hydrogel to purify seawater, a desalination experiment was carried out on seawater (Bohai Sea, China), where inductively coupled plasma optical emission spectroscopy (ICP-OES) was used to determine the concentrations of Na^+, Mg^{2+}, Ca^{2+}, K^+ in the seawater and condensed water. In addition, 20 mg L^{-1} of methyl blue solution was used to simulate printing and dyeing wastewater, and the absorbance of the purified water was measured at 326 nm using a UV-Vis spectrophotometer (UH4150, Hitachi, Japan) to explore the adsorption capacity of the hydrogels.

3. Results and discussion

3.1 Morphological characterization and structural analysis

The pure cellulose hydrogel (CG) is white (Fig. S1a), which is disadvantageous for light absorption whereas the addition of polypyrrole (PPy) causes the hydrogels to turn black (Fig. S1b). The hydrogels, PCGs, are porous with pore sizes ranging from tens to hundreds of micrometers, which is beneficial to water transport (Fig. 2a-d). The insets show that the in-situ PPy-coated PCGs are rough which enlarges the specific surface area and sunlight scattering [40]. Moreover, with the increase of cellulose content, the hydrogel pore size gradually decreases (Figure S2), which is expected to have detrimental effect on the water transport performance. After tensile elongation to

~200% and compression loading by 300 g the PCG2 sample regains its original dimensions , demonstrating high elastic limit of the hydrogel (Fig. S3).

To explore the chemical structure of the hydrogels, they are along with their constituents examined by Fourier transformed infrared spectroscopy (FTIR) as shown in Figure 2e. In the PPy spectrum (dark blue curve), the peaks located at 1616 cm^{-1} and 1467 cm^{-1} are assigned to the intra-ring stretching of the C=C of the pyrrole ring [39, 41]. In addition, the peaks at 1200 cm^{-1} and 1049 cm^{-1} represent the C-N stretching vibration band and the in-plane bending vibration of the pyrrole ring N-H bond, respectively [39, 40]. The spectrum of CG (green curve) exhibits signals at 1631 cm^{-1} and 1400 cm^{-1}, ascribed to the stretching vibration of -C=O and bending vibration of C-H. The broad absorption peak located at 3000-3500 cm^{-1} corresponds to surface hydroxyl groups. In the spectra of PCGs, the carbonyl stretching signal is shifted to 1616 cm^{-1} from 1631 cm^{-1}, which is ascribed to the formation of hydrogen bonds between PPy and the cellulose matrix. The disappearance of the C-N stretching peak at 1200 cm^{-1} for the composite hydrogels is attributed to the formation of hydrogen bonds and peak overlap [40]. XRD spectra reveal that the cellulose crystal structure is unaffected by PPy doping, which can explain the synthesized hydrogels retaining the cellulose porous framework (Figure S4).

To further understand the chemical interactions in the hydrogel network, its rheological behavior is studied (Fig 2f). The storage modulus (G') of the hydrogel is higher than the loss modulus (G"), indicating significant viscoelastic solid-state characteristics. More importantly, G' of PCG2 is higher than CG, demonstrating that the composite hydrogel network forms additional interactions in the hydrogel than in the absence of PPy. All in all, the PCG composite hydrogel has high mechanical strength and good thermal stability, which originates from the synergistic effect of PPy and cellulose, which as identified by rheological experiment and thermogravimetric analysis (TG, STA 409, NETZSCH, Germany) (Figure S5).

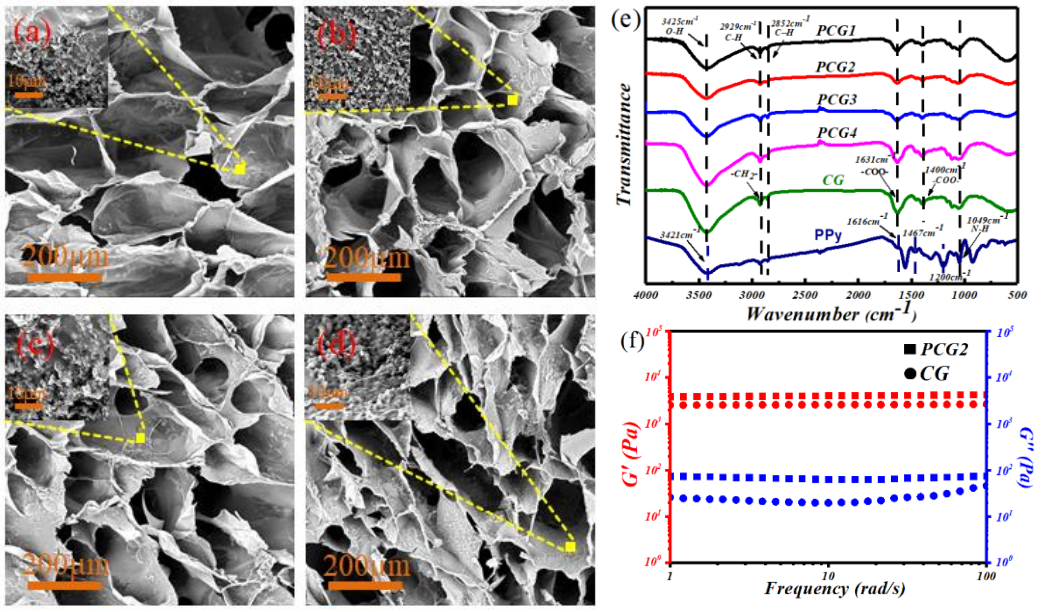

Figure 2. SEM images of (a-d) polypyrrole cellulose hydrogels. The solid content of cellulose is 2.5 wt%, 3 wt%, 3.5 wt% and 4 wt%, in PCG1, PCG2, PCG3 and PCG4, respectively. (e) FTIR spectrum of PPy, CG and PCGs with different solid content. (f) Dynamic mechanical analysis of CG and PCG2 hydrogels.

3.2 Light absorption performance and surface wettability

With the structure of the hydrogels appearing suitable for the application, focus is turned to the optical properties that are investigated by ultraviolet-visible-near infrared (UV-Vis-NIR) spectroscopy in the wavelength range of 300-2500 nm, as shown in Fig. 3a. The absorbance of pure CG is modest (about 44%), whereas the PCG samples exhibit a solar spectral absorption above 90%, with PCG2 having the highest absorption of 95%. The improved absorption upon addition of polypyrrole is ascribed to its the broad and strong light absorption. Complementary to light absorption properties, the hydrogel hydrophilicity affects the water evaporation and water transport rate. The contact angle of the hydrophilic CG is 19.1°, amid the high hydroxyl density. The contact angle of PCG1 to PCG4 gradually increases from 32.3° to 47.3° that is when the amount of cellulose and PPy increases with a fixed ratio between cellulose and PPy. Hence, it is inferred that PPy dominates the hydrophilicity of the hydrogel. (Fig. 3b). Nonetheless, PCGs are still hydrophilic, laying the foundation for solar steam generation.

Efficient thermal management is especially important for the thermal localization effect of solar evaporators to combat heat loss. The surface temperature of the PCG2 hydrogel under one sun

irradiation has been monitored using an infrared thermal imager (Fig. 3c and d). The surface equilibrium temperature of the composite hydrogel increases from 22.8°C to 43.8°C in 30 min, indicating that the evaporator has superior thermal management performance compared to previous studies (Table S2). The thermal conductivities of CG and PCG2 in wet state has been measured to 0.24 W m^{-1} K^{-1} and 0.38 W m^{-1} K^{-1}, respectively, which is lower than pure water (0.59 W m^{-1} K^{-1}), as shown in Fig. 3e. The low thermal conductivities of the hydrogels are due to water molecules being restricted by hydrogen bonds to the hydrogel membrane, which prevents water flow between the hydrogel cavities [42]. This ultimately reduces the heat loss from the hydrogels. The PCG2 sample has a higher conductivity than CG as the polypyrrole is a known good electrical conductor and according to the Wiedemann-Franz equation hence also thermal conductor.

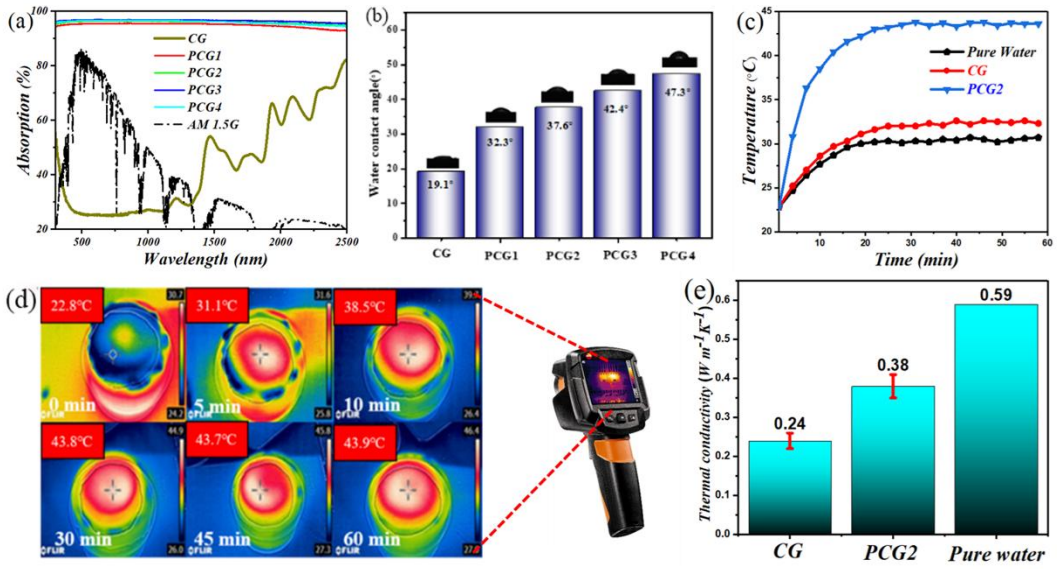

Figure 3. (a) Light absorption spectra of hydrogels with and without PPy in the range 300-2500 nm. (b) Water contact angles of CG and PCGs samples. (c) Temperature profiles of CG, PCG2 and water from 0 to 60 min under one sun irradiation. (d) Infrared camera images showing the temperature distribution in PCG2 during 60 min. (e) Thermal conductivity of CG, PCG2 and water.

3.3 Adjustable water transport performance

Owing to the intermolecular hydrogen bond differences, the water of the hydrated polymer network is divided into three types: free water, intermediate water and bound water [41]. The interaction between the intermediate water and the polymer chain is weak [39], leading to low evaporation enthalpy, with the amount of intermediate water controlled by the expansion capacity

of the hydrable polymer network. The reduced evaporation enthalpy means that water molecules are more likely to break the intermolecular hydrogen bonds and escape from the liquid water film during solar evaporation, resulting in efficient water evaporation [43]. Therefore, to demonstrate the evaporation enthalpy reduction through the polymer network, differential scanning calorimetry (DSC) is employed, as shown in Fig. 4a. Compared to pure water, the evaporation occurs from lower temperatures in the hydrogels, which reveal that the evaporation of water in the composite hydrogels is different from the evaporation of the bulk water. Since the experiments are carried out in the same environment, according to [35],

$$E_{equ}=E_0 m_0/m_g \quad (1)$$

the equivalent water evaporation enthalpy (E_{equ}) in the PCGs samples can be calculated from the evaporation enthalpy (E_0), mass change (m_0) of pure water and the mass change of the hydrogel (m_g) (For details see Note S1) [41]. The enthalpy reduction of the hydrogels is in the range 595-834 J/g with PCG2 exhibiting the highest reduction (Fig. 4b and Table S1). Increasing cellulose solid content, provides increased hydroxyl group density in the hydrogel network, which increases the content of intermediate water to yield a lower evaporation enthalpy. However, further increase of the solid content as in the PCG4 sample, causes increased hydrophobicity (Figure 3b) reducing the amounts of intermediate water in the polymer network and hence reduces the enthalpy. In addition, the melting behavior of PCGs samples at low temperature was also performed to further investigate the interaction of water states in hydrogels, as shown in Figure S8.

Since the hydrophilic groups of the polymer network can strongly interact with water molecules, the proportion of intermediate water in the hydrogels can be adjusted by changing the hydratable polymer network, and hence, the content of intermediate water can be expressed by the saturated water content (Q_s) [35]. Q_s can be calculated by the following formula,

$$Q_s=W/W_d \quad (2)$$

where W and W_d are the weights of water in the fully swollen sample and the corresponding dry hydrogel sample, respectively. A high porosity generally supports the saturated water content, prompting more water to be heated by the solar energy, which in turn has the drawback of increased heat loss and concomitantly reduced the evaporation rate and efficiency. As the hydrogel water equilibrium under ambient conditions, is around half of the saturated value, the water content of

PCG is reduced to its half-saturated state, $0.5Q_s$, by using absorbent paper. The half-swelling time, the duration from half to fully saturated, is quantified as the hydrogel is almost fully saturated during steam generation. The water transport rate is calculated as,

$$V=0.5Q_s/t \qquad (3)$$

where t is the swelling time from $0.5Q_s$ to Q_s. The Q_s values of PCG1 to PCG4 are 19.3, 15.26, 12.19 and 8.26 g g^{-1}, respectively, which correlates with the contact angle measurements (Fig. 4c). Combined with the half-swollen time, the water transport rates (V) of the PCGs composite hydrogels is determined to 0.77, 0.51, 0.33 and 0.183 g min^{-1}, respectively (Fig. 4d). Inferior water transfer rates inflict a decrease in evaporation rate, while too high water transfer rate relative to the evaporation rate increases the water content of the hydrogel which causes more solar energy to be consumed for water heating (heat loss) and therefore intermediate water transfer rates are expected to yield the optimum overall performance.

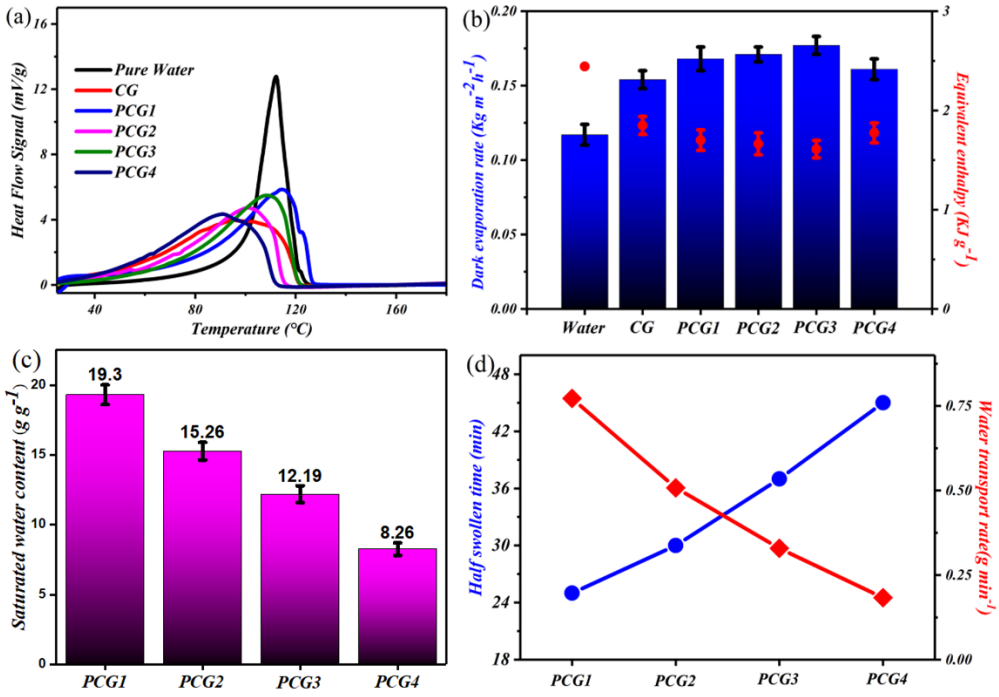

Figure 4. (a) DSC curves of CG, PCGs and water as reference. (b) Water evaporation rates and corresponding equivalent evaporation enthalpy of CG and PCGs in dark environment. (c) Saturated water content of PCGs sample in dry state. (d) Swelling properties and water transport capacity of PCGs (Left axis: time from semi-swollen state to swollen state of hydrogel; Right axis: water transport rate).

3.4 Solar evaporation

As the applicability of the material in solar evaporation depends on the parameters described in the above, water transport rate, saturation levels, hydrogen bonding capacity and the fact that some of these parameters are negatively correlated, it is necessary to perform actual evaporation experiments to quantify the influence of the hydrogel structure on the water evaporation capacity.

A solar simulator is used to mimic vertical sunlight on the hydrogel evaporator and the spot size is adjusted to the size of the hydrogel sample. As shown in Figure S6, PCG-0.3 has the highest evaporation rate of 1.65 kg m^{-2} h^{-1}, which correlates with dark evaporation experiments showing that this hydrogel also has the lowest evaporation enthalpy of 1729 J g^{-1} (Figure 5a). With low content of PPy, the energy utilization of the composite hydrogel is insufficient, however, with increased loading of PPy, the thermal conductivity increases, which causes conduction and convective heat loss of the photothermal film. Therefore, a PPy optimum exists and in the present study, the optimal ratio of immobilized PPy and cellulose appears to be 0.3:1. Hence, the solid content of the hydrogel is fixed for this PPy-cellulose ratio to study the impact of the solid content on the evaporation performance of the composite hydrogels (Fig. 5b). According to the slope of the curve, the evaporation rates of pure water, CG, PCG1, PCG2, PCG3 and PCG4 are 0.36 kg m^{-2} h^{-1}, 0.80 kg m^{-2} h^{-1}, 1.57 kg m^{-2} h^{-1}, 1.88 kg m^{-2} h^{-1}, 1.65 kg m^{-2} h^{-1} and 1.68 kg m^{-2} h^{-1} (Fig. 5c), respectively. The highest evaporation rate is thus found for PCG2 and is 5.16 times that of pure water and 2.33 times that of CG and the evaporation rate is higher than in previously reported studies [5, 22, 24, 25, 38, 40, 42, 44-47]. Compared with PCG2, PCG1 has larger pores and higher water transmission rate, which leads to more solar energy being used to heat the bottom water, which increases the heat loss. The lower evaporation rates of PCG3 and PCG4 can be attributed to insufficient water transport capacity, limiting the evaporation process, whereas in PCG2, the water transport rate and evaporation rate are balanced. Moreover, the evaporation potential of the hydrogels is evaluated by calculating the solar conversion efficiency (η) according to the following equation [48],

$$\eta = m h_{LV} / C_{opt} P_0 \qquad (4)$$

Where m is the evaporation rate (evaporation rate in dark environment has been subtracted), h_{LV} is the water evaporation enthalpy in the composite hydrogel, C_{opt} is the concentration, and P_0 is the

sunlight intensity (1 kW m^{-2}). The evaporation efficiency of PCG2 is 87.89% compared to 41.08% for CG, demonstrating the influence of the PPy (Fig. 5d). Under natural conditions, the sunlight intensity is lower than the one sun radiation (<1 kW m^{-2}) and thus the evaporation efficiency and rate of the hydrogel under different irradiation intensities is explored, as shown in Fig. 5e. Under a sunlight intensity of 0.5 kW m^{-2}, the evaporation rate of PCG2 is 0.936 kg m^{-2} h^{-1}, which remains superior to that of pure water (0.357 kg m^{-2} h^{-1} under 1.0 sun), showing the applicability of composite hydrogel in natural environments.

In the process of seawater evaporation, salt can crystallise in the porous structure of the hydrogel, which eventually leads to the paralysis of the evaporator. In order to evaluate the salt-tolerance of hydrogel, Eq 5 is utilized in order to deduct the salt content from the evaporation enthalpy as an increased salt concentration naturally leads to less water content and thus lower evaporation rate,

$$m_s = m'/\omega_{water} \qquad (5)$$

where m' represents the evaporation rates of the hydrogel at different salt concentrations under one sun illumination (Fig. S7), and ω_{water} denotes the mass fraction of water in the brine sample. The m_s values of PCG2 remain around 1.85 at the brine concentrations of 3.5 wt%, 7 wt% and 10 wt%. When the salt concentration reaches 20 wt%, the m_s value is 1.825, which is on the border of being outside the experimental uncertainty, but as the evaporation rate remains unchanged during the 1h experiment, it is inferred that evaporator is unaffected by brine concentrations up to 20%. In addition, the equivalent evaporation enthalpy of PCG2 sample at different salt concentrations in dark environment is also investigated (Table 1). Correlated for the salt concentration, the water evaporation enthalpy is constant, implying that the hydrogen bonding capacity is unaffected by the increased ionic strength of the brine. Meanwhile, it is found that the PCG2 evaporator has a stable evaporation rate after 20 consecutive cycles (2 h per cycle) under one sun, reflecting long-term durability (Fig. 5f). After placing 1g of salt on the surface of the hydrogel, the salt particles gradually disappear during the evaporation process at 3.5 wt% brine, which is ascribed to the highly hydrated porous hydrogel triggering diffusive dissolution of salt ions to the underneath body water through capillary pumping and concentration difference. However, the automatic NaCl cleaning leads to contraction of the hydrogel, which could be caused by the formation of inter and intramolecular

complexes between Na^+ and polyhydroxy groups, and possibly enhanced electrostatic attraction between the anionic sites of the polymer chains and Na^+, causing enhanced ionic cross-linking and increased rigidity of the hydrogel [49].

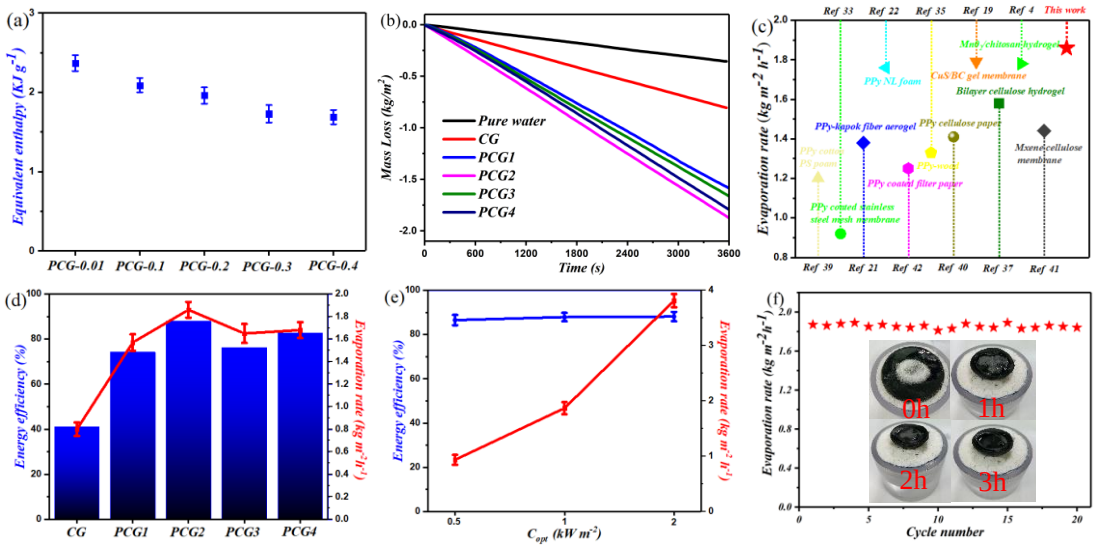

Figure 5. (a) Equivalent evaporation enthalpy of PPy/cellulose hydrogels with different mass ratios measured in dark environment. (b) Water mass loss curves of the composite hydrogels under one sun illumination. (c) Evaporation rates of PCG2 evaporator compared to other doped PPy absorbers or hydrogel evaporators under one sun illumination. (d) Energy conversion efficiency and evaporation rate of composite hydrogels under one sun. (e) Energy conversion efficiency and evaporation rate of PCG2 under light intensities of 0.5, 1 and 2 kW m^{-2}. (f) Evaporation rate of PCG2 in 3.5 wt% brine after 20 consecutive cycles under one sun. The inset shows the disappearance of salt particles on the evaporator surface during 3h.

Table 1. Evaporation rate and enthalpy of PCG2 hydrogel at different salt concentrations.

	Pure water	3.5wt%	7wt%	10wt%	20wt%
m_s	1.876	1.855	1.849	1.844	1.825
Dark experiment ($J\ g^{-1}$)	1664	2097	2174	2365	2355

3.5 Desalination and water purification

In addition to the solar steam generation capability, the performance of the composite hydrogel membranes in seawater desalination is investigated to broaden their application field. Hence, a seawater desalination device is built outdoors, where a composite hydrogel sample with a surface

area of 200×150 mm^2 floating on the seawater surface of the evaporation device is employed and the collected condensed water is weighed to evaluate steam production (Fig. 6a). The temperature and solar flux changes over the time range from 9:00 to 17:00 are recorded in Fig. 6b (May 3, 2022, Tiangong University, China). The sunlight intensity fluctuates in the range of 0.3~0.76 kW m^{-2} and the corresponding ambient temperature increases from 20 °C to 28 °C and then drops to 24 °C. The evaporation rate ranges from 0.4 to 0.91 kg m^{-2} h^{-1}, which is lower than the evaporation rate under laboratory conditions of half a sun. As shown in Fig. 6c, four ion concentrations (Na^+, Mg^{2+}, Ca^{2+} and K^+) in the condensed water desalted by the PCG2 composite hydrogel are monitored by ICP-OES. The ion concentrations decrease by 5 orders of magnitude (ion rejection ratio above 99.9%), providing ion concentrations below those of membrane based (10-500 mg L^{-1}) and distillation based (1-50 mg L^{-1}) seawater desalination [1] and more than 2 orders of magnitude below the 200 mg/L drinking water standard set by the World Health Organization.

A previous study shows that while the porous structure of pure CG has certain adsorption capacity for printing and dyeing wastewater, it lacks the catalytic activity under natural sunlight and its methylene blue (MB) removal capabilities are negligible [31]. As shown in Fig. 6d, a methylene blue solution is used to simulate printing and dyeing wastewater to evaluate the wastewater purification capacity of PCG2. The visible light absorbance of the cleaned water is almost zero, and the hydrogel water purification capacity is comparable to that of photocatalyst-added hydrogels and exceeds that of most hydrogel materials (Table S2). The water cleaning capability of the hydrogels has a dual origin. First, the porous structure of the composite hydrogel and the roughness conferred by PPy provide a higher specific surface area, resulting in increased dye adsorption [31]. Second, The abundant hydroxyl groups in the cellulose matrix can form hydrogen bonds with the tertiary amines and sulfonic oxygen atoms of organic dyes, which further enhances the adsorption effect [26].

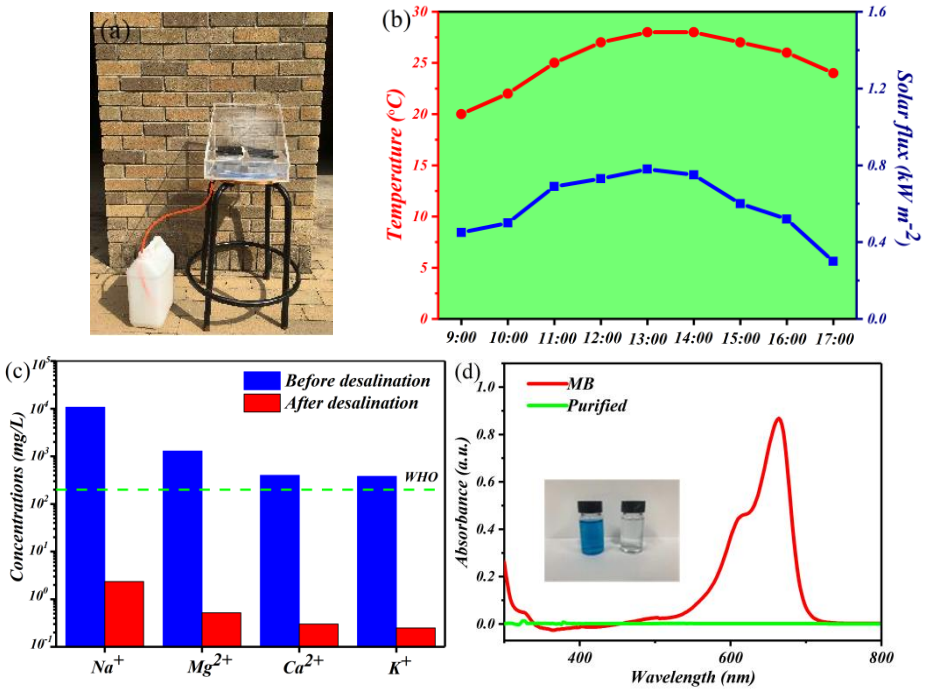

Figure 6. (a) Outdoor solar evaporation device for seawater desalination. (b) Temperature and solar flux of the evaporation device under natural sunlight exposure during the experiment. (c) Concentrations of Na^+, Mg^{2+}, Ca^{2+} and K^+ in the seawater and in condensed water collected by the PCG2-based solar device after evaporation are compared with seawater ion concentrations. (d) UV-Vis spectroscopic analysis of methyl blue (MB) solution treated by PCG2 (purified).

4. Conclusion

In this paper, an air-water interface solar evaporator comprising a cellulose-based composite hydrogel as the evaporation layer is designed. The hydrogel is created from cellulose coated by in-situ polymerized poolypyrrole (PPy). Due to the broad light absorption of PPy also providing hydrophobic evaporation sites and the hydrophilic porous structure of cellulose itself that weakens the intermolecular water bonds, the prepared hydrogels have a high evaporation rate and solar energy conversion efficiency. By changing the solid content of cellulose and PPy, the amount of intermediate water (water with reduced evaporation ethalpy) is increased, and the swelling ability of the hydrogel can be tailored to reduce the overall water evaporation enthalpy, which greatly promotes solar water evaporation as balanced water transport and evaporation rate are paramount for high efficiency which is optimized to 87.89% and the evaporation rate is unaffected by salt concentrations up to 20%. In addition, the composite hydrogel evaporator is used in seawater desalination and an ion rejection rate of the obtained condensate is 99%. The evaporator has long-

term durability demonstrated by unaffected evaporation rate after twenty test cycles on pure water. Further, the ability to remove dyes from printing and dyeing wastewater, exemplified by methylene blue, is demonstrated as the light absorbance of the cleaned water obtained is zero. Overall, the synthesized hydrogels combine mechanical strength, evaporation performance, applicability and scalability for the next-generation water purification applications.

Conflict of interest

There is no conflict of interest for this manuscript.

Acknowledgments

This work was supported by the National Key Research and Development Program of China (No. 2016YFB 0303000) and the New Materials Research Key Program of Tianjin (No. 16ZXCL GX00090).

References

[1] Geng Y, Zhang K, Yang K, Ying P, Hu L, Ding J, Xue J, Sun W, Sun K, Li M (2019) Constructing hierarchical carbon framework and quantifying water transfer for novel solar evaporation configuration. Carbon 155:25-33. https://doi.org/10.1016/j.carbon.2019.08.055

[2] Liu X, Cheng H, Guo Z, Zhan Q, Qian J, Wang X (2018) Bifunctional, moth-eye-like nanostructured black titania nanocomposites for solar-driven clean water generation. ACS Appl Mater Interfaces 10:39661-39669. https://doi.org/10.1021/acsami.8b13374

[3] Li Y, Tao R, Yang Z, Fan Y, Bian T, Fan X, Su C, Shao Z (2022) Cuprous oxide single-crystal film assisted highly efficient solar hydrogen production on large ships for long-term energy storage and zero-emission power generation. J Power Sources 527:231133. https://doi.org/10.1016/j.jpowsour.2022.231133

[4] Wang Y, Wan Y, Meng X, Jiang L, Wei H, Zhang X, Ma N (2022) Bio-inspired MXene coated wood-like ordered chitosan aerogels for efficient solar steam generating devices. J Mater Sci 57:13962-

13973. https://doi.org/10.1007/s10853-022-07494-0

[5] Irshad MS, Wang X, Abbasi MS, Arshad N, Chen Z, Guo Z, Yu L, Qian J, You J, Mei T (2021) Semiconductive, flexible MnO_2 NWs/chitosan hydrogels for efficient solar steam generation. ACS Sustain Chem Eng 9:3887-3900. https://doi.org/10.1021/acssuschemeng.0c08981

[6] Ni G, Li G, Boriskina SV, Li H, Yang W, Zhang T, Chen G (2016) Steam generation under one sun enabled by a floating structure with thermal concentration. Nat Energy 1:1-7. https://doi.org/10.1038/nenergy.2016.126

[7] Wei W, Guan Q, You C, Yu J, Yuan Z, Qiang P, Zhou C, Ren Y, You Z, Zhang F (2020) Highly compact nanochannel thin films with exceptional thermal conductivity and water pumping for efficient solar steam generation. J Mater Chem A 8:13927-13934. https://doi.org/10.1039/d0ta02921a

[8] Tao P, Ni G, Song C, Shang W, Wu J, Zhu J, Chen G, Deng T (2018) Solar-driven interfacial evaporation. Nat Energy 3:1031-1041. https://doi.org/10.1038/s41560-018-0260-7

[9] Zhou L, Tan Y, Wang J, Xu W, Yuan Y, Cai W, Zhu S, Zhu J (2016) 3D self-assembly of aluminium nanoparticles for plasmon-enhanced solar desalination. Nat Photonics 10:393-398. https://doi.org/10.1038/nphoton.2016.75

[10] Zhu M, Li Y, Chen F, Zhu X, Dai J, Li Y, Yang Z, Yan X, Song J, Wang Y, Hitz E, Luo W, Lu M, Yang B, Hu L (2018) Plasmonic wood for high-efficiency solar steam generation. Adv Energy Mater 8:33-41. https://doi.org/10.1002/aenm.201701028

[11] Ibrahim I, Seo DH, Angeloski A, McDonagh A, Shon HK, Tijing LD (2021) 3D microflowers CuS/Sn_2S_3 heterostructure for highly efficient solar steam generation and water purification. Sol Energ Mat Sol C 232:111377. https://doi.org/10.1016/j.solmat.2021.111377

[12] Yu F, Ming X, Xu Y, Chen Z, Meng D, Cheng H, Shi Z, Shen P, Wang X (2019) Quasimetallic molybdenum carbide–based flexible polyvinyl alcohol hydrogels for enhancing solar water evaporation. Adv Mater Interfaces 6:1901168. https://doi.org/10.1002/admi.201901168

[13] Li Y, Wang Z, Tao R, Fan Y, Xu J, Yu L, Ren N, Wu J, Chen D, Shao Z (2021) Preparation strategies of p-type cuprous oxide and its solar energy conversion performance. Energ Fuel 35:17334-17352. https://doi.org/10.1021/acs.energyfuels.1c02777

[14] Liu Y, Chen J, Guo D, Cao M, Jiang L (2015) Floatable, self-cleaning, and carbon-black-based superhydrophobic gauze for the solar evaporation enhancement at the air-water interface. ACS Appl

Mater Interfaces 7:13645-13652. https://doi.org/10.1021/acsami.5b03435

[15] Fang W, Zhao L, Chen H, He X, Li W, Du X, Sun Z, Zhang T, Shen Y (2019) Graphene oxide foam fabricated with surfactant foaming method for efficient solar vapor generation. J Mater Sci 54:12782-12793. https://doi.org/10.1007/s10853-019-03794-0

[16] Li W, Tian X, Li X, Liu J, Li C, Feng X, Shu C, Yu ZZ (2022) An environmental energy-enhanced solar steam evaporator derived from MXene-decorated cellulose acetate cigarette filter with ultrahigh solar steam generation efficiency. J Colloid Interface Sci 606:748-757. https://doi.org/10.1016/j.jcis.2021.08.043

[17] Zou Y, Yang P, Yang L, Li N, Duan G, Liu X, Li Y (2021) Boosting solar steam generation by photothermal enhanced polydopamine/wood composites. Polymer 217:123464. https://doi.org/10.1016/j.polymer.2021.123464

[18] Li X, Xu W, Tang M, Zhou L, Zhu B, Zhu S, Zhu J (2016) Graphene oxide-based efficient and scalable solar desalination under one sun with a confined 2D water path. P Natl Acad Sci USA 113:13953-13958. https://doi.org/10.1073/pnas.1613031113

[19] Ma Y, Jiang T, Zhang A, Cao J (2021) Spent coffee ground-based interfacial solar steam generation. J Mater Cycles Waste 23:604-613. https://doi.org/10.1007/s10163-020-01148-6

[20] Liu X, Hou B, Wang G, Cui Z, Zhu X, Wang X (2018) Black titania/graphene oxide nanocomposite films with excellent photothermal property for solar steam generation. J Mater Res 33:674-684. https://doi.org/10.1557/jmr.2018.25

[21] Wang G, Fu Y, Guo A, Mei T, Wang J, Li J, Wang X (2017) Reduced graphene oxide-polyurethane nanocomposite foam as a reusable photoreceiver for efficient solar steam generation. Chem Mater 29:5629-5635. https://doi.org/10.1021/acs.chemmater.7b01280

[22] Zhang D, Cai Y, Liang Q, Wu Z, Sheng N, Zhang M, Wang B, Chen S (2020) Scalable, flexible, durable, and salt-tolerant CuS/bacterial cellulose gel membranes for efficient interfacial solar evaporation. ACS Sustain Chem Eng 8:9017-9026. https://doi.org/10.1021/acssuschemeng.0c01707

[23] Yang Y, Liu C, Zhao M, Wang J, Tian X (2021) Highly efficient solar steam generation under low solar flux via carbon-nanotube-modified sugarcane. Energy Technol-Ger 9: 2100588. https://doi.org/10.1002/ente.202100588

[24] Mu P, Bai W, Fan Y, Zhang Z, Sun H, Zhu Z, Liang W, Li A (2019) Conductive hollow kapok fiber-

PPy monolithic aerogels with excellent mechanical robustness for efficient solar steam generation. J Mater Chem A 7:9673-9679. https://doi.org/10.1039/c8ta12243a

[25] Xu Y, Wang J, Yu F, Guo Z, Cheng H, Yin J, Yan L, Wang X (2020) Flexible and efficient solar thermal generators based on polypyrrole coated natural latex foam for multimedia purification. ACS Sustain Chem Eng 8:12053-12062. https://doi.org/10.1021/acssuschemeng.0c03164

[26] Guo Y, Lu H, Zhao F, Zhou X, Shi W, Yu G (2020) Biomass-derived hybrid hydrogel evaporators for cost-effective solar water purification. Adv Mater 32:e1907061. https://doi.org/10.1002/adma.201907061

[27] Yu Y, Zhu X, Wang L, Wu F, Liu S, Chang C, Luo X (2020) A simple strategy to design 3-layered Au-TiO_2 dual nanoparticles immobilized cellulose membranes with enhanced photocatalytic activity. Carbohydr Polym 231:115694. https://doi.org/10.1016/j.carbpol.2019.115694

[28] Zou Y, Wu X, Li H, Yang L, Zhang C, Wu H, Li Y, Xiao L (2021) Metal-phenolic network coated cellulose foams for solar-driven clean water production. Carbohydr Polym 254:117404. https://doi.org/10.1016/j.carbpol.2020.117404

[29] Erdal NB, Hakkarainen M (2022) Degradation of cellulose derivatives in laboratory, man-made, and natural environments. Biomacromolecules 23:2713-2729. https://doi.org/10.1021/acs.biomac.2c00336

[30] Fang H, Feng N, Wu D, Hu D (2021) Design and fabrication of epichlorohydrin-cross-linked methyl cellulose aerogel-based composite materials for magnetic UV response light-to-heat conversion and storage. Biomacromolecules 22:4155-4168. https://doi.org/10.1021/acs.biomac.1c00650

[31] Chen Y, Xiang Z, Wang D, Kang J, Qi H (2020) Effective photocatalytic degradation and physical adsorption of methylene blue using cellulose/GO/TiO_2 hydrogels. RSC Adv 10:23936-23943. https://doi.org/10.1039/d0ra04509h

[32] Macruz PD, Nippes RP, de Matos Jorge LM, dos Santos OAA (2022) Photocatalytic removal of persistent pollutants using eco-friendly ZnO. J Solgel Sci Technol 104:387-400. https://doi.org/10.1007/s10971-022-05949-z

[33] Marra M, Dumont M, Palhares HG, Alcamand HA, Houmard M, Nunes EHM (2022) Structural and photocatalytic properties of sol–gel-derived TiO_2 samples prepared by conventional and hydrothermal methods using a low amount of water. J Solgel Sci Technol 103:97-107.

https://doi.org/10.1007/s10971-022-05780-6

[34] Zhou X, Guo Y, Zhao F, Yu G (2019) Hydrogels as an emerging material platform for solar water purification. Acc Chem Res 52:3244-3253. https://doi.org/10.1021/acs.accounts.9b00455

[35] Zhou X, Zhao F, Guo Y, Zhang Y, Yu G (2018) A hydrogel-based antifouling solar evaporator for highly efficient water desalination. Energ & Environ Sci 11:1985-1992. https://doi.org/10.1039/c8ee00567b

[36] Guo Y, Zhao X, Zhao F, Jiao Z, Zhou X, Yu G (2020) Tailoring surface wetting states for ultrafast solar-driven water evaporation. Energ & Environ Sci 13:2087-2095. https://doi.org/10.1039/d0ee00399a

[37] Hanif Z, Tariq MZ, Khan ZA, La M, Choi D, Park SJ (2022) Polypyrrole-coated nanocellulose for solar steam generation: A multi-surface photothermal ink with antibacterial and antifouling properties. Carbohydr Polym 292:119701. https://doi.org/10.1016/j.carbpol.2022.119701

[38] Zhang L, Tang B, Wu J, Li R, Wang P (2015) Hydrophobic light-to-heat conversion membranes with self-healing ability for interfacial solar heating. Adv Mater 27:4889-4894. https://doi.org/10.1002/adma.201502362

[39] Zhao F, Zhou X, Shi Y, Qian X, Alexander M, Zhao X, Mendez S, Yang R, Qu L, Yu G (2018) Highly efficient solar vapour generation via hierarchically nanostructured gels. Nat Nanotechnol 13:489-495. https://doi.org/10.1038/s41565-018-0097-z

[40] Huang W, Hu G, Tian C, Wang X, Tu J, Cao Y, Zhang K (2019) Nature-inspired salt resistant polypyrrole–wood for highly efficient solar steam generation. Sustain Energ Fuels 3:3000-3008. https://doi.org/10.1039/c9se00163h

[41] Zhou X, Zhao F, Guo Y, Rosenberger B, Yu G (2019) Architecting highly hydratable polymer networks to tune the water state for solar water purification. Sci Adv 5:eaaw5484. https://doi.org/10.1126/sciadv.aaw5484

[42] Hu N, Xu Y, Liu Z, Liu M, Shao X, Wang J (2020) Double-layer cellulose hydrogel solar steam generation for high-efficiency desalination. Carbohydr Polym 243:116480. https://doi.org/10.1016/j.carbpol.2020.116480

[43] Lu Y, Fan D, Wang Y, Xu H, Lu C, Yang X (2021) Surface patterning of two-dimensional nanostructure-embedded photothermal hydrogels for high-yield solar steam generation. ACS Nano 15:10366-10376. https://doi.org/10.1021/acsnano.1c02578

[44] Hao D, Yang Y, Xu B, Cai Z (2018) Efficient solar water vapor generation enabled by water-absorbing polypyrrole coated cotton fabric with enhanced heat localization. Appl Therm Eng 141:406-412. https://doi.org/10.1016/j.applthermaleng.2018.05.117

[45] Xu Y, Liu D, Xiang H, Ren S, Zhu Z, Liu D, Xu H, Cui F, Wang W (2019) Easily scaled-up photo-thermal membrane with structure-dependent auto-cleaning feature for high-efficient solar desalination. J Membrane Sci 586:222-230. https://doi.org/10.1016/j.memsci.2019.05.068

[46] Zha XJ, Zhao X, Pu JH, Tang LS, Ke K, Bao RY, Bai L, Liu ZY, Yang MB, Yang W (2019) Flexible anti-biofouling MXene/cellulose fibrous membrane for sustainable solar-driven water purification. ACS Appl Mater Interfaces 11:36589-36597. https://doi.org/10.1021/acsami.9b10606

[47] Zhang Y, Cao S, Qiu Z, Yin K, Lei Y, Sun K, Chang X, Li X, Fan R (2019) In situ chemo-polymerized polypyrrole-coated filter paper for high-efficient solar vapor generation. Int J Energ Res 44:1191-1204. https://doi.org/10.1002/er.5012

[48] Wei D, Wang F, Sun H, Zhu Z, Liang W, Li A (2021) Ionic hyper-cross-linked polymers monoliths for efficient solar steam generation. Eur Polym J 147:110281. https://doi.org/10.1016/j.eurpolymj.2021.110281

[49] Yu J, Yang G, Li Y, Yang W, Gao J, Lu Q (2014) Synthesis, characterization, and swelling behaviors of acrylic acid/carboxymethyl cellulose superabsorbent hydrogel by glow-discharge electrolysis plasma. Polym Eng Sci 54:2310-2320. https://doi.org/10.1002/pen.23791